

Design rules for modulation-doped AlAs quantum wells

Yoon Jang Chung, K. W. Baldwin, K. W. West, D. Kamburov, M. Shayegan, and L. N. Pfeiffer

Department of Electrical Engineering, Princeton University, Princeton, New Jersey 08544, USA

(Received 24 April 2017; revised manuscript received 12 June 2017; published 17 July 2017)

Owing to their multivalley, anisotropic, energy band structure, two-dimensional electron systems (2DESs) in modulation-doped AlAs quantum wells (QWs) provide a unique platform to investigate electron interaction physics and ballistic transport. Indeed, a plethora of phenomena unseen in other 2DESs have been observed over the past decade. However, a foundation for sample design is still lacking for AlAs 2DESs, limiting the means to achieve optimal quality samples. Here, we present a systematic study on the fabrication of modulation-doped AlAs and GaAs QWs over a wide range of $\text{Al}_x\text{Ga}_{1-x}\text{As}$ barrier alloy compositions. Our data indicate clear similarities in modulation doping mechanisms for AlAs and GaAs, and provide guidelines for the fabrication of very high quality AlAs 2DESs. We highlight the unprecedented quality of the fabricated AlAs samples by presenting the magnetotransport data for low-density ($\simeq 1 \times 10^{11} \text{ cm}^{-2}$) AlAs 2DESs that exhibit high-order fractional quantum Hall signatures.

DOI: [10.1103/PhysRevMaterials.1.021002](https://doi.org/10.1103/PhysRevMaterials.1.021002)

Clean two-dimensional electron systems (2DESs) which exhibit the fractional quantum Hall effect are ideal systems to study electron-electron interaction phenomena and many-body ground states. Along with the classic example of modulation-doped GaAs [1,2], recent studies have revealed that we can add AlAs [3–15], Si [16,17], Ge [18], ZnO [19], and graphene [20] to the list of materials in which high-order fractional states have been observed. The AlAs system is particularly exciting. First, its lattice constant closely matches that of GaAs, therefore allowing the growth of very high quality single-crystal AlAs epitaxial layers on GaAs substrates. Second, as shown in Fig. 1, AlAs distinguishes itself from GaAs in where its conduction-band electrons are in the first Brillouin zone. In bulk AlAs, electrons occupy multiple conduction-band minima (valleys) with anisotropic energy versus wave-vector dispersions. When electrons are confined to an AlAs quantum well (QW), by varying the well-width and in-plane strain, one can make the 2D electrons occupy the valleys with different (in-plane) anisotropies, effective mass, and effective Landé g -factors [10]. These different parameters, and the flexibility to control the valley occupation, render the AlAs 2DES a unique system for probing exotic many-body as well as ballistic transport phenomena. Recent studies in AlAs 2DESs have indeed led to the observation of integer and fractional quantum Hall ferromagnetism [4,14], valley skyrmion formation [7], and interaction-enhanced valley susceptibility for electrons [8,10] and composite fermions [11]; it was also reported recently that the transport anisotropy of electrons is transferred to the composite fermions in AlAs QWs [13]. The AlAs 2DES is also a prime candidate for “valleytronic” devices [21], and it was the first system where ballistic electron transport in different valleys was demonstrated [6,9]. Despite the abundance of literature concerning the rich physics of 2DESs in AlAs QWs, there are fundamental unanswered questions about modulation doping in these systems. For example, over an extended period of time, many studies on AlAs QWs have utilized $\text{Al}_x\text{Ga}_{1-x}\text{As}$ barrier alloy fractions in the vicinity of $x \simeq 0.40$ [3–15]. This choice is based on the fact that at this x the minima of the Γ and X bands are known to cross, hence providing the maximum conduction-band offset for populating the AlAs QW. However, as is well known for

the case of GaAs QWs, maximum conduction-band offset does not necessarily relate to the best sample quality because of factors such as interface quality or background impurities in the barrier [22,23]. As shown in Fig. 1(c), since the barrier material flanking an AlAs QW is similar to what flanks a GaAs QW except that the band minimum is the X band rather than the Γ band, we could expect similar behavior for AlAs QWs. However, because there have not been many studies on barrier alloy fractions other than $x \simeq 0.40$, it is difficult to assess these possibilities. Here, we provide guidelines to grow modulation-doped AlAs QWs, flanked by $\text{Al}_x\text{Ga}_{1-x}\text{As}$ barriers with $0.20 \leq x \leq 0.80$. By deducing the relevant energy levels from electron density measurements, we find that the modulation doping characteristics of AlAs and GaAs QWs are essentially identical. Our data show that this is true over the entire range of x , where three different situations can occur for the conduction-band alignment of the two types of QWs considering both the Γ and X bands, as shown in Fig. 2. Because modulation doping is a thermal equilibrium process, no fundamental distinction is observed when comparing cases that involve both the X and Γ bands [Figs. 2(a) and 2(f)] with the single X -band (Γ -band) processes in Figs. 2(b) and 2(c) [Figs. 2(d) and 2(e)]. We highlight this fact by demonstrating high-quality modulation-doped AlAs QWs with $x = 0.33$. For our study, AlAs or GaAs QWs, flanked by $\text{Al}_x\text{Ga}_{1-x}\text{As}$ barriers with δ -Si doping, were grown by molecular beam epitaxy on (001) GaAs substrates [see Fig. 1(d)]. We use a Si doping concentration ranging from $\simeq 3 \times 10^{11}$ to $1 \times 10^{12} \text{ cm}^{-2}$ for the substrate side, and ~ 1.5 – 2 times this value on the surface side. The lower limit is implemented to prevent parallel conduction in the $x \leq 0.26$ AlAs QWs. The growth temperature was measured by a factory calibrated optical pyrometer (Ircan Modline 7V-1205, emissivity set to 0.63) and was fixed to be $645 \text{ }^\circ\text{C}$ for all samples at all times except for when δ doping the 2 nm $\text{Al}_x\text{Ga}_{1-x}\text{As}$ layer beneath the lower spacer of the QWs, where the temperature was lowered to $480 \text{ }^\circ\text{C}$ to prevent surface segregation of the Si [24–27]. The x ranged from 0.20 to 0.80 for the AlAs QWs and 0.26 to 1.0 for the GaAs QWs. We examined reflection high-energy electron diffraction patterns prior the growth of each sample to determine compositions

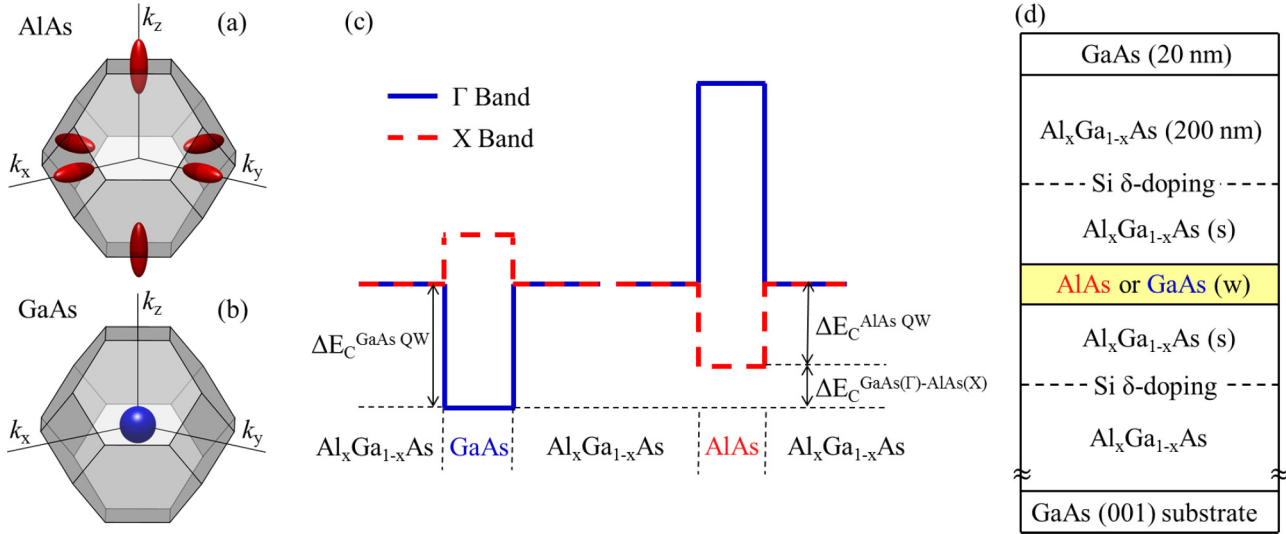


FIG. 1. The first Brillouin zones and electron Fermi surfaces of bulk (a) AlAs and (b) GaAs. (c) Comparison of the conduction-band diagrams near GaAs and AlAs quantum wells. (d) The sample structure implemented in this work, with w and s denoting well width and spacer thickness, respectively

and growth rates. Well-width (w) and spacer thicknesses (s) were fixed at 11 and 59 nm for the AlAs QWs and 20 and

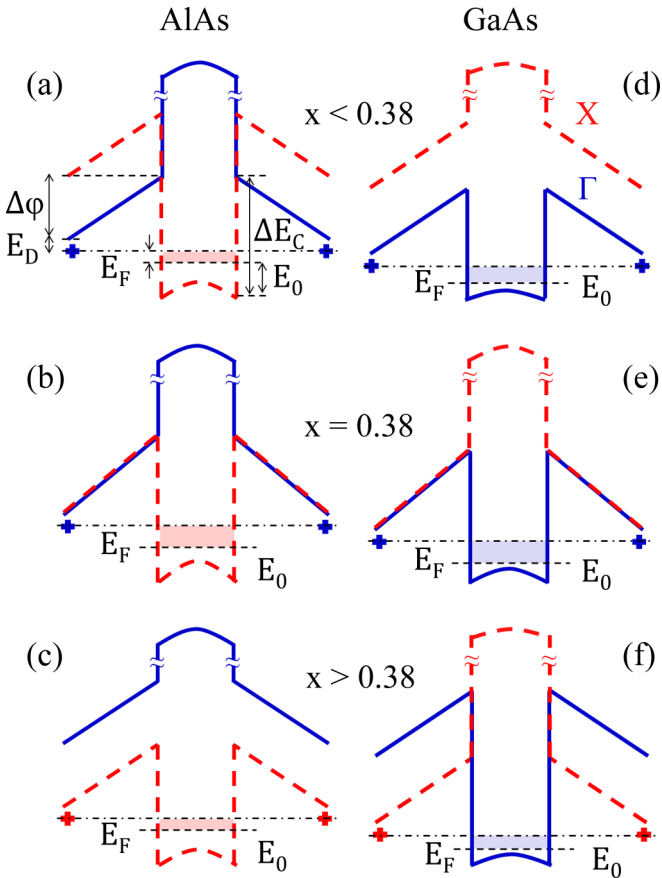


FIG. 2. Schematic diagrams of the conduction band in the vicinity of (a)–(c) AlAs and (d)–(f) GaAs quantum wells for barrier alloy fractions $x < 0.38$, $x = 0.38$, and $x > 0.38$. The dashed red and solid blue lines represent the X-band and Γ -band edges, respectively.

70 nm for the GaAs QWs. For measurements we used a low-frequency lock-in technique and a pumped ^3He cryostat with a base temperature of 0.3 K. Magnetoresistance data were taken by sweeping a superconducting magnet from 0 to 14.5 T in the dark and after illuminating the sample with a red light emitting diode at ~ 10 K. Before presenting the experimental data, we briefly describe the valley occupation and parameters for our AlAs 2DESs. In AlAs QWs with $w \gtrsim 5$ nm, biaxial compression from epitaxial growth on GaAs substrates raises the ground-state energy of the valley with its major axis along the growth direction, causing the other two (in-plane) valleys to be occupied [10]. Our AlAs QWs have a well width in this regime and thus have in-plane effective mass values of $m_l^* = 1.1m_e$ and $m_t^* = 0.20m_e$, with a geometric mean of $m^* = \sqrt{m_l^*m_t^*} = 0.45m_e$, and an out-of-plane mass of $m_t^* = 0.20m_e$ (m_e is the free electron mass). Figure 3(a) shows the density of electrons (n) for our AlAs and GaAs QWs as a function of x . All electron concentration values were evaluated from the quantum Hall features in the magnetotransport data. Although there is an offset between the density profiles for the two QWs, it is clear that the variations in n for GaAs and AlAs QWs have a similar trend with x for measurements both taken in the dark and after light illumination. As we elaborate below, this suggests a common mechanism for the modulation doping of the two QWs. It is important to note here that at higher barrier alloy fractions ($x \geq 0.38$), an annealing technique [12] is required to achieve saturated carrier concentrations after illumination. Different annealing conditions are needed for saturation for different x , with $x = 0.38$ having the longest time constant of the order of 1 h at ~ 40 K. For $x \leq 0.33$, the extra annealing step was unnecessary, likely because the time constant is short enough so that the process is completed during the ~ 30 min it takes to cool the illuminated sample from 10 to 0.3 K in our system [28]. This behavior is observed for both GaAs and AlAs wells, corroborating our conclusion that the modulation dopings into these wells share a universal mechanism. Using the textbook model for modulation-doped

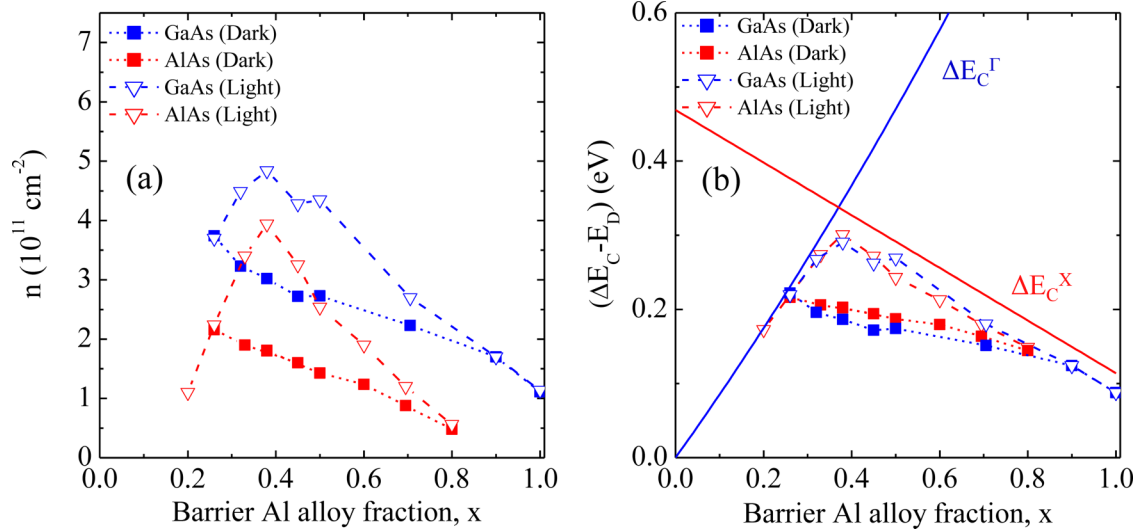


FIG. 3. (a) Measured electron densities for the AIAs and GaAs QWs as a function of x . The squares represent densities measured in the dark while the triangles show data points after light exposure; the lines are guides to the eye. The well-width and spacer thicknesses are 11 and 59 nm for the AIAs and 20 and 70 nm for the GaAs samples. (b) Values of $(\Delta E_C - E_D)$ deduced from the experimental data points of (a) for the AIAs and GaAs QW samples (see text). The solid blue and red lines show our estimates for the Γ - and X -band edge energies relative to the Γ -band edge of GaAs.

heterostructures [29], we can relate our measured n with the energy levels of the QW,

$$\Delta E_C = E_0 + E_F + E_D + \Delta\varphi, \quad (1)$$

where E_0 is the ground-state energy measured relative to the conduction-band edge of the QW, E_F is the Fermi level measured with respect to E_0 , E_D is the donor level energy defined relative to the conduction-band edge of the barrier, and $\Delta\varphi \equiv ns e^2 / \epsilon_b$ [see Fig. 2(a)]. Here, ϵ_b is the barrier dielectric constant and e is the electron charge. Using values of n and s we can determine $\Delta\varphi$ and $E_F = n\pi\hbar^2 / g_v m^*$, where \hbar is the Planck constant and m^* is the effective mass in the QW ($m^* = 0.067m_e$ for GaAs and $m^* = 0.45m_e$ for AIAs); g_v is the valley degeneracy ($g_v = 1$ for GaAs and $g_v = 2$ for AIAs). From the simple case of an infinite potential well, we can also get a rough estimate for E_0 , which is ≈ 15 meV for the AIAs QWs ($m_t^* = 0.2m_e$, $w = 11$ nm) and ≈ 14 meV for the GaAs QWs ($m^* = 0.067m_e$, $w = 20$ nm). Considering, as an example, the case of the GaAs QW with $x = 0.33$ and $n = 4.5 \times 10^{11} \text{ cm}^{-2}$ after illumination, we deduce $\Delta\varphi \approx 238$ meV, and $E_F \approx 16$ meV. Since E_0 and E_F are both much smaller than $\Delta\varphi$, we conclude from Eq. (1) that $\Delta\varphi \approx (\Delta E_C - E_D)$. Implementing a self-consistent Schrödinger-Poisson solver corrects E_0 of the order of ≈ 5 – 10 meV. More precise calculations require an exact knowledge of ΔE_C for all alloy fractions, but this would not alter the relation $\Delta\varphi \approx (\Delta E_C - E_D)$ which is the crucial factor in understanding the design rules in this study. The symbols in Fig. 3(b) show the values of $(\Delta E_C - E_D)$, with respect to the Γ -band edge of GaAs, deduced from the density data points in Fig. 3(a) and using Eq. (1) assuming E_0 values of an infinite potential well. To account for the fact that the conduction-band minima of AIAs QWs are not aligned with GaAs QWs, we take the offset between GaAs(Γ) and AIAs(X) to be 114 meV [30] and add this constant value to all the $(\Delta E_C - E_D)$ values for the AIAs QWs. Since the calculated $\Delta\varphi$ is ≈ 70 meV for our AIAs/GaAs/AIAs (i.e.,

$x = 1$) structure, and previous reports quote shallow donor energies in AIAs ranging from ≈ 30 to 60 meV [31–33], the value of 114 meV we take from the literature is quite consistent with our results. It is seen in Fig. 3(b) that with the 114 meV offset there is excellent agreement between the $(\Delta E_C - E_D)$ values for the AIAs and GaAs QWs over the entire range of x . From our data points measured after illumination, we can estimate the conduction-band offset with respect to GaAs(Γ) for $\text{Al}_x\text{Ga}_{1-x}\text{As}$ in modulation-doped structures, drawn as the solid blue and red lines for the Γ and X bands in Fig. 3(b). For the Γ band, the $x < 0.38$ data coincide very well with the reported literature values of the conduction-band offset ΔE_C^Γ [34,35] assuming a hydrogenic donor level. For the X band we draw a line that goes through the reported GaAs(X)-GaAs(Γ) offset value of ≈ 470 meV [34] and our expected AIAs(X)-GaAs(Γ) offset of 114 meV. We find there is reasonable agreement with the data in Fig. 3(b), including the Γ - X band crossing point in $\text{Al}_x\text{Ga}_{1-x}\text{As}$ at $x = 0.38$. The deep donor levels measured from the data in the dark agree well with previous reports on the DX effect in $\text{Al}_x\text{Ga}_{1-x}\text{As}$ [31,36], showing a maximum effective barrier near $x = 0.26$ and monotonic decrease when $x > 0.26$. We also comment on the mobility values measured for our samples. Figures 4(a) and 4(b) show the mobility values as a function of carrier concentration for the AIAs and GaAs samples, respectively. Note that for the AIAs samples at any given density, the measured mobility is higher than in previous studies [5,12], attesting to the high quality of the samples used in our study. This is particularly impressive considering that, in contrast to the samples in Ref. [5], our samples are doped from both sides and have smaller spacer thicknesses. The power law fit for the relation between density and mobility yields $\mu \propto n^{1.4}$ for the AIAs QWs and $\mu \propto n^3$ for the GaAs QWs. We postulate that the notable deviation from the well-known $\mu \propto n^{1.5}$ for the GaAs samples is due to significant contributions from the barrier in the two lowest-density samples, where $x = 1.0$

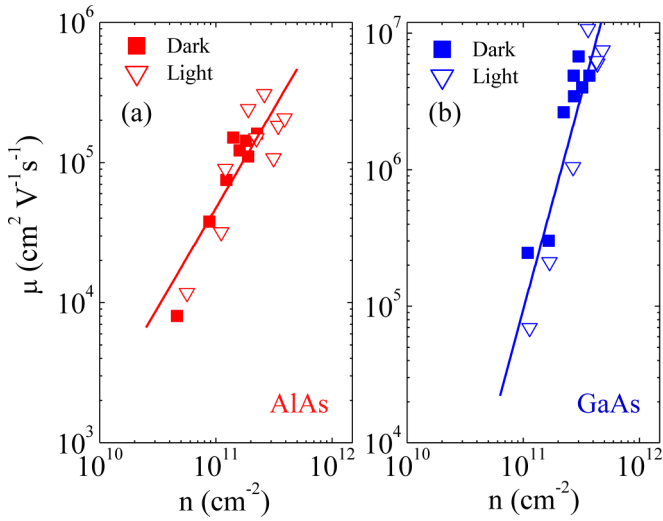


FIG. 4. Measured mobility values for the (a) AlAs and (b) GaAs QWs in our study. The power law fits correspond to a relation of $\mu \propto n^{1.4}$ for the AlAs QWs and $\mu \propto n^3$ for the GaAs QWs.

and 0.9. Indeed, if we perform a fit while omitting the data from these two samples, we achieve a power law of $\mu \propto n^{1.6}$. These results suggest that barrier quality is also an important factor to consider in sample optimization, as mentioned earlier in the introduction. To evaluate the potential of high quality AlAs samples with $x < 0.38$, we grew a set of AlAs QWs with $x = 0.33$ and varying spacer thicknesses. Figures 5(a)–5(c) show longitudinal magnetoresistance (R_{xx}) data for the $x = 0.33$ AlAs wells with spacer thicknesses of 59, 136, and 178 nm, respectively. The dependence of n on

spacer thickness is plotted in the inset of Fig. 4(a), which clearly shows that it is governed by the $n \propto s^{-1}$ relation expected of modulation-doped structures. The indices A–F in Figs. 5(a)–5(c) and the inset mark the corresponding densities of each trace. Figures 5(a)–5(c) demonstrate the high quality of the fabricated samples, with clear indications of the 2/3 and 1/3 fractional quantum Hall states (FQHSs) even at the low density of $6.1 \times 10^{10} \text{ cm}^{-2}$ (F) for the 178 nm spacer sample [Fig. 5(c)]. After light exposure, n for this sample increases to $1.2 \times 10^{11} \text{ cm}^{-2}$ (E), and the measured trace shows excellent quality with clear R_{xx} minima at filling factors $\nu = 2/3, 3/5, 4/7, 3/7,$ and $2/5$. The $s = 59 \text{ nm}$ sample, which has a higher density of $3.4 \times 10^{11} \text{ cm}^{-2}$ (A) after light, also shows FQHSs at $\nu = 5/3$ and $4/3$. We emphasize that all of these samples were fabricated with $x = 0.33$, and were measured after a brief illumination of $\sim 1 \text{ min}$ (with a current of 6 mA in the light emitting diode) at 10 K and a subsequent cooldown to 0.3 K after the light was turned off, with no additional procedures such as annealing [12] or gating [5]. The results presented here suggest that when the conditions of the barrier are dominant in determining the quality of the AlAs 2DESs, we can resort to the conventional techniques used for GaAs to implement small x barriers. For example, in GaAs samples with sufficiently large s , the intentional ionized impurities are far enough from the 2DES that the scattering term from the unintentional (background) impurities in the barrier becomes significant, and hence having a small x barrier is crucial for a high quality due to the inherently more reactive nature of Al compared to Ga. If we extend this concept to AlAs QWs, it suggests that in low-density AlAs 2DES where s is large, we should grow AlAs QWs with small x for optimal performance. This could also apply to narrow AlAs QWs, where the significant penetration of the electron wave function

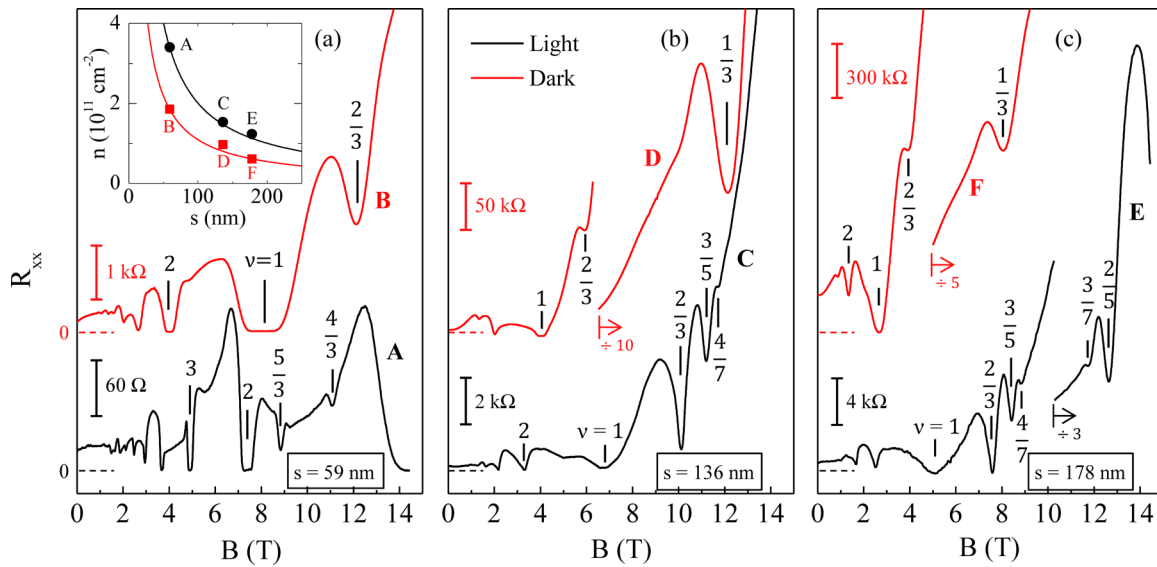


FIG. 5. (a)–(c) Representative magnetotransport (R_{xx}) traces measured at 0.3 K in the dark and after illumination for AlAs QW structures with spacer thicknesses of 59, 136, and 178 nm. The inset in (a) shows the electron density vs spacer thickness, with solid lines representing the expected values for $n \propto s^{-1}$ [see Eq. (1)]. The scales for the resistance axes are given for each trace with dashed lines denoting zero. The Landau level filling factors (ν) for some of the integer and fractional quantum Hall states are marked in each trace. The indices of A–F in the inset to (a) are given to mark the corresponding electron densities of each trace; these densities are A: 3.4, B: 1.9, C: 1.5, D: 9.7, E: 1.2, F: 0.61, all in units of 10^{11} cm^{-2} .

into the barrier again makes it beneficial to have a barrier with small x . In conclusion, our measurements of the electron density in modulation-doped AIAs and GaAs QWs over a wide range of $\text{Al}_x\text{Ga}_{1-x}\text{As}$ barrier alloy fractions reveal that their doping characteristics are essentially identical despite having different electron pocket distributions in the Brillouin zone. We highlight this by the observation of the $n \propto s^{-1}$ rule for $x = 0.33$ AIAs wells with 59, 136, and 178 nm spacer thicknesses. Our fabricated AIAs QWs show high quality magnetotransport data with clear indications of FQHSs. The

design rules we establish here for modulation-doped GaAs and AIAs QWs provide a foundation for application in specific sample optimization, especially in the case of AIAs, which was so far a relatively uncharted material compared to GaAs.

We acknowledge support through the NSF (Grants No. DMR 1305691 and No. ECCS 1508925) for measurements, and the NSF (Grant No. MRSEC DMR 1420541) and the Gordon and Betty Moore Foundation (Grant No. GBMF4420) for sample fabrication and characterization.

-
- [1] D. C. Tsui, H. L. Stormer, and A. C. Gossard, Two-Dimensional Magnetotransport in the Extreme Quantum Limit, *Phys. Rev. Lett.* **48**, 1559 (1982).
- [2] W. Pan, H. L. Stormer, D. C. Tsui, L. N. Pfeiffer, K. W. Baldwin, and K. W. West, Transition From an Electron Solid to the Sequence of Fractional Quantum Hall States at Very Low Landau Level Filling Factor, *Phys. Rev. Lett.* **88**, 176802 (2002).
- [3] T. S. Lay, J. J. Heremans, Y. W. Suen, M. B. Santos, K. Hirakawa, M. Shayegan, and A. Zrenner, High-quality two-dimensional electron system confined in an AIAs quantum well, *Appl. Phys. Lett.* **62**, 3120 (1993).
- [4] E. P. De Poortere, E. Tutuc, S. J. Papadakis, and M. Shayegan, Resistance spikes at transitions between quantum Hall ferromagnets, *Science* **290**, 1546 (2000).
- [5] E. P. De Poortere, Y. P. Shkolnikov, E. Tutuc, S. J. Papadakis, M. Shayegan, E. Palm, and T. Murphy, Enhanced electron mobility and high order fractional quantum Hall states in AIAs quantum wells, *Appl. Phys. Lett.* **80**, 1583 (2002).
- [6] O. Gunawan, Y. P. Shkolnikov, E. P. De Poortere, E. Tutuc, and M. Shayegan, Ballistic Electron Transport in AIAs Quantum Wells, *Phys. Rev. Lett.* **93**, 246603 (2004).
- [7] Y. P. Shkolnikov, S. Misra, N. C. Bishop, E. P. De Poortere, and M. Shayegan, Observation of Quantum Hall “Valley Skyrmions,” *Phys. Rev. Lett.* **95**, 066809 (2005).
- [8] O. Gunawan, Y. P. Shkolnikov, K. Vakili, T. Gokmen, E. P. De Poortere, and M. Shayegan, Valley Susceptibility of an Interacting Two-Dimensional Electron System, *Phys. Rev. Lett.* **97**, 186404 (2006).
- [9] O. Gunawan, B. Habib, E. P. De Poortere, and M. Shayegan, Quantized conductance in an AIAs two-dimensional electron system quantum point contact, *Phys. Rev. B* **74**, 155436 (2006).
- [10] M. Shayegan, E. P. De Poortere, O. Gunawan, Y. P. Shkolnikov, E. Tutuc, and K. Vakili, Two-dimensional electrons occupying multiple valleys in AIAs, *Phys. Status Solidi B* **243**, 3629 (2006).
- [11] N. C. Bishop, M. Padmanabhan, K. Vakili, Y. P. Shkolnikov, E. P. De Poortere, and M. Shayegan, Valley Polarization and Susceptibility of Composite Fermions Around a Filling Factor $\nu = 3/2$, *Phys. Rev. Lett.* **98**, 266404 (2007).
- [12] S. Dasgupta, C. Knaak, J. Moser, M. Bichler, S. F. Roth, A. F. i Morral, G. Abstreiter, and M. Grayson, Donor binding energy and thermally activated persistent photoconductivity in high mobility (001) AIAs quantum wells, *Appl. Phys. Lett.* **91**, 142120 (2007).
- [13] T. Gokmen, M. Padmanabhan, and M. Shayegan, Transference of transport anisotropy to composite fermions, *Nat. Phys.* **6**, 621 (2010).
- [14] M. Padmanabhan, T. Gokmen, and M. Shayegan, Ferromagnetic Fractional Quantum Hall States in a Valley-Degenerate Two-Dimensional Electron System, *Phys. Rev. Lett.* **104**, 016805 (2010).
- [15] A. V. Shchepetilnikov, Y. A. Nefyodov, I. V. Kukushkin, L. Tiemann, C. Reichl, W. Dietsche, and W. Wegscheider, Electron g -factor anisotropy in an AIAs quantum well probed by ESR, *Phys. Rev. B* **92**, 161301(R) (2015).
- [16] K. Lai, W. Pan, D. C. Tsui, S. Lyon, M. Mühlberger, and F. Schäffler, Two-Flux Composite Fermion Series of the Fractional Quantum Hall States in Strained Si, *Phys. Rev. Lett.* **93**, 156805 (2004).
- [17] T. M. Kott, B. Hu, S. H. Brown, and B. E. Kane, Valley-degenerate two-dimensional electrons in the lowest Landau level, *Phys. Rev. B* **89**, 041107R (2014).
- [18] Q. Shi, M. A. Zudov, C. Morrison, and M. Myronov, Spinless composite fermions in an ultrahigh-quality strained Ge quantum well, *Phys. Rev. B* **91**, 241303R (2015).
- [19] A. Tsukazaki, S. Akasaka, K. Nakahara, Y. Ohno, H. Ohno, D. Maryenko, A. Ohtomo, and M. Kawasaki, Observation of the fractional quantum Hall effect in an oxide, *Nat. Mater.* **9**, 889 (2010).
- [20] C. R. Dean, A. F. Young, P. Cadden-Zimansky, L. Wang, H. Ren, K. Watanabe, T. Taniguchi, P. Kim, J. Hone, and K. L. Shepard, Multicomponent fractional quantum Hall effect in graphene, *Nat. Phys.* **7**, 693 (2011).
- [21] A. Rycerz, J. Tworzydło, and C. W. J. Beenakker, Valley filter and valley valve in graphene, *Nat. Phys.* **3**, 172 (2007).
- [22] M. Shayegan, V. J. Goldman, M. Santos, T. Sajoto, L. Engel, and D. C. Tsui, Two-dimensional electron system with extremely low disorder, *Appl. Phys. Lett.* **53**, 2080 (1988).
- [23] S. D. Sarma and E. H. Hwang, Mobility versus quality in two-dimensional semiconductor structures, *Phys. Rev. B* **90**, 035425 (2014).
- [24] A. M. Santos, T. Sajoto, A. Zrenner, and M. Shayegan, Effect of Substrate Temperature on Migration of Si in planar-doped GaAs, *Appl. Phys. Lett.* **53**, 2504 (1988); **55**, 603(E) (1989).
- [25] A. M. Lanzilotto, M. Santos, and M. Shayegan, A SIMS study of the migration of Si in planar-doped GaAs and $\text{Al}_{0.25}\text{Ga}_{0.75}\text{As}$, *Appl. Phys. Lett.* **55**, 1445 (1989).
- [26] A. M. Lanzilotto, M. Santos, and M. Shayegan, Silicon migration during the molecular beam epitaxy of delta-doped GaAs and $\text{Al}_{0.25}\text{Ga}_{0.75}\text{As}$, *J. Vac. Sci. Technol.* **A8**, 2009 (1990).
- [27] L. Pfeiffer, E. F. Schubert, K. W. West, and C. W. Magee, Si dopant migration and the AlGaAs/GaAs inverted interface, *Appl. Phys. Lett.* **58**, 2258 (1991).

- [28] J. Chen, C. H. Yang, R. A. Wilson, and M. J. Yang, Observation of negative persistent photoconductivity in an n -channel GaAs/Al $_x$ Ga $_{1-x}$ As single heterojunction, *Appl. Phys. Lett.* **60**, 2113 (1992).
- [29] J. H. Davies, *The Physics of Low Dimensional Semiconductors* (Cambridge University Press, Cambridge, UK, 1997).
- [30] J. M. Smith, P. C. Klipstein, R. Grey, and G. Hill, Resonant tunneling between transverse X states in GaAs/AlAs double-barrier structures under elevated hydrostatic pressure, *Phys. Rev. B* **57**, 1740 (1998).
- [31] N. Chand, T. Henderson, J. Klem, W. T. Masselink, R. Fischer, Y. Chang, and H. Morkoç, Comprehensive analysis of Si-doped Al $_x$ Ga $_{1-x}$ As ($x = 0$ to 1): Theory and experiments, *Phys. Rev. B* **30**, 4481 (1984).
- [32] S. Adachi, GaAs, AlAs, and Al $_x$ Ga $_{1-x}$ As: Material parameters for use in research and device applications, *J. Appl. Phys.* **58**, R1 (1985).
- [33] H. J. Lee, L. Y. Juravel, J. C. Woolley, and A. J. S. Thorpe, Electron transport and band structure of Ga $_{1-x}$ Al $_x$ As alloys, *Phys. Rev. B* **21**, 659 (1980).
- [34] L. Pavesi and M. Guzzi, Photoluminescence of Al $_x$ Ga $_{1-x}$ As alloys, *J. Appl. Phys.* **75**, 4779 (1994).
- [35] J. Batey and S. L. Wright, Energy band alignment in GaAs:(Al, Ga)As heterostructures: The dependence on alloy composition, *J. Appl. Phys.* **59**, 200 (1986).
- [36] D. J. Chadi and K. J. Chang, Energetics of DX -center formation in GaAs and Al $_x$ Ga $_{1-x}$ As alloys, *Phys. Rev. B* **39**, 10063 (1989).